NMH-CS 3.0: a C# Programming Language and Windows System based Ecohydrological Model Derived from Noah-MP

Yong-He Liu[1], Zong-Liang Yang[2]

[1] School of Resources and Environment, Henan Polytechnic University, Jiaozuo, Henan, China

[2] Jackson School of Geoscience, University of Texas at Austin, Austin TX, USA

Correspondence: Yong-He Liu (yonghe_hpu@163.com)

Abstract. The community Noah with multi-parameterization options (Noah-MP) land surface model (LSM) is widely used in studies from uncoupled land surface hydrometeorology and ecohydrology to coupled weather and climate predictions. In this study, we developed NMH-CS 3.0, a hydrological model written in CSharp(C#). NMH-CS 3.0 is a new model developed by faithfully translating the FORTRAN version Noah-MP from the uncoupled WRF-Hydro 3.0, and is coupled with a river routing model. NMH-CS has the capacity of execution on Windows systems, utilizing the multi-core CPUs commonly available in today's personal computers. The code of NMH-CS has been tested to ensure that it produces a high-degree of consistency with the output of the original WRF-Hydro. High-resolution (6 km) simulations were conducted and assessed over a grid domain covering the entire Yellow River Basin and the most of North China. The spatial maps and temporal variations of many state variables simulated by NMH-CS 3.0 and WRF-Hydro/Noah-MP demonstrate highly consistent results, with occasionally minor discrepancies. The river discharge for the Yellow River simulated by the new model with various scheme combinations of six parameterizations exhibit general agreement with the natural river discharge at the Lanzhou station. NMH-CS can be regarded as a reliable replica of Noah-MP in WRF-Hydro 3.0, but it can leverage the modern, powerful, and user-friendly features brought by the C# language to significantly improve the efficiency of the model users and developers.

1 Introduction.

In contemporary hydrological prediction and flood warning applications, the effectiveness of hydrological models hinges on their ability to delineate intricate energy and water processes on the land surface, surpassing the capabilities of traditional rainfall-runoff models. To address this demand, certain land surface models (LSMs) utilized by atmospheric science communities have been bolstered with hydrological simulation features, as observed in WRF-Hydro (Lin et al., 2018), or conventional rainfall-runoff models have been enriched with more comprehensive descriptions of land surface processes, exemplified by the VIC model (Liang et al., 1994).

The Noah Land Surface Model with multi-parameterizations (Noah-MP) (Niu et al., 2011; Yang et al., 2011) stands out as a robust tool for studying global water issues, serving as the foundation for models like WRF-Hydro, which incorporates Noah-MP (Gochis, 2020). However, the code for Noah-MP and WRF-Hydro is written in FORTRARN, a 'legacy' language, posing challenges for code analysis and editing, unlike more modern languages such as CSharp(C#), because FORTRAN lacks the similar

intelligent efficient programming tools that are now common for C#. This limitation makes it arduous for users unfamiliar with FORTRAN to efficiently comprehend and modify the code. Additionally, Noah-MP and WRF-Hydro necessitate a UNIX-like operating system, causing inconvenience for the users and developers relying on Windows systems. Therefore, there is a compelling need to code Noah-MP in a contemporary modern programming language, to gain a wider accessibility of the Noah-MP model.

We designed NMH-CS 3.0, a Noah-MP based Hydrological model coded using the CSharp (C#) programming language. This model was crafted by creating a framework and accurately translating the original Noah-MP LSM code from WRF-Hydro 3.0 and coupling with a Muskingum method-based river routing model(Liu et al., 2023). C#, recognized for its modern and object-oriented approach, is widely used for software development across various platforms, particularly on the Windows operating system. According to the TIOBE Programming Community Index (https://www.tiobe.com/) for October 2024, C# ranks fifth among major programming languages with a user base of 5.6%, while Fortran ranks ninth with only 1.8% of users.

NMH-CS provides several advantages over the original WRF-Hydro/Noah-MP. Unlike the original version that requires compiling for each computer and primarily depends on Unix-like systems, NMH-CS can seamlessly run on Windows systems that support the Microsoft Dotnet Framework. The executable files, once compiled, can be easily packaged and distributed to other Windows machines, offers greater convenience for users who are less familiar with Unix-like operations. The utilization of the C# language facilitates advanced software tools for visualizing and analyseing the model's code, enhancing the convenience for users to read, modify and debug the code. This is appealing to the model developers who are proficient in C# language and the object-oriented programming. The design of NMH-CS aligns with the input datasets and configurations specified in the 'namelist' file, ensuring high compatibility with WRF-Hydro 3.0. Leveraging the parallel computing capabilities of C#, both the translated Noah-MP LSM simulation and the river routing simulation within NMH-CS support parallel execution on common personal computers.

2 The Noah-MP LSM

Noah-MP is a robust model renowned for its capability to represent diverse physical processes. Since its initial introduction (Niu et al., 2011) (Yang et al., 2011), Noah-MP has been widely used. For example, Noah-MP has been coupled to WRF-Hydro as a major module, and can be seamlessly integrated into the Weather Research and Forecasting (WRF) model (Gochis, 2020). Furthermore, the offline WRF-Hydro model plays a pivotal role in the National Water Model, contributing to the simulation of floods and river flows across the United States (Bales, 2019) (Francesca et al., 2020) (Karki et al., 2021). Noah-MP's versatility extends to applications such as streamflow prediction (Lin et al., 2018) and the estimation of evapotranspiration, surface temperature, carbon fluxes, heat fluxes, and soil moisture, as demonstrated in many studies (Chang et al., 2020; Gao et al., 2015; Li et al., 2022; Ma et al., 2017; Yang et al., 2021). Noah-MP is supported by several different modelling frameworks to facilitate coupling it to various earth system framework models including HRLDAS (Chen et al., 2007), LIS(Kumar et al., 2006), and WRF-Hydro(Gochis, 2020). This makes Noah-MP a powerful research and forecasting tool within the hydrology community.

Noah-MP excels in physical representation of water and energy dynamics across various environmental layers, including a vegetation canopy layer, multiple snow and soil layers, and an optional unconfined

79 aquifer layer for groundwater. To capture specific physical processes, Noah-MP employs multiple
80 parameterization schemes, providing users the flexibility to choose from a total of 12 parametrizations,
81 as detailed in Table 1. This versatility enables tailored representation of diverse environmental conditions
82 and processes, enhancing the model's adaptability and applicability.
83
84
85 **Table 1:** Parameterization options for Noah-MP (an asterisk (*) denotes the recommended default
86 option). Certain abbreviations correspond to terms used for Parameterization Schemes (PS) in Noah-
87 MP, and their meanings can be referenced in the WRF-Hydro 3.0 user document (Gochis et. al., 2015).
88 Note that these options may not be applicable to other versions of Noah-MP, such as that used in
89 HRLDAS. The scheme options here are presented by some abbreviation marks such as 'Noah' or
90 Schaake96 are those used in the 'namelist' file for Noah-MP.

Abbreviation	Physical parameterization	Scheme Code	Scheme Options
DVEG	Vegetation option	1~5	*1 table LAI, read FVEG; 2 dynamic LAI, FVEG=f(LAI); 3 table LAI, FVEG=f(LAI); 4 table LAI, FVEG=maximum; 5 dynamic LAI, FVEG =maximum
CRS	Stomatal conductance (controls transpiration from leaves)	1~2	*1 Ball-Berry; 2 Jarvis
BTR	β-factor (soil moisture stress factor controlling transpiration)	1~3	*1 Noah; 2 CLM; 3 SSiB
RUN	Runoff (runoff generation at and below the surface)	1~4	1 SIMGM; 2 SIMTOP; *3 Schaake96; 4 BATS
SFC	Surface layer drag coefficient	1~2	*1 M-O; 2 Chen97
FRZ	Frozen soil permeability	Fixed to 2	*1 NY06; 2 Koren99
INF	Supercooled liquid water	Fixed to 2	*1 NY06; 2 Koren99
RAD	Radiation transfer option	1~3	1 gap=F(3D,cosz); 2 gap=0; *3 gap=1-Fveg
ALB	Snow surface albedo	Fixed to 2	1 BATS; *2 CLASS
SNF	Precipitation partition option (rainfall or snowfall)	Fixed to 2	*1 Jordan91; 2 BATS; 3 Noah
TBOT	Lower boundary of soil temperature	1~2	*1 zero-flux; 2 Noah
STC	Snow/soil temperature time scheme	Fixed to 1	*1 semi-implicit; 2 fully implicit; 3 Ts=f(fsno)

91

92 **3 Development of NMH-CS**

93 **3.1 Translation of Noah-MP Code**

94 Our primary focus in developing NMH-CS involves translating the original FORTRAN code of Noah-
95 MP into the C# language. It is essential to note that this translation is based on a relatively older version

96   of Noah-MP utilized in WRF-Hydro 3.0, as the process was started before the release of Noah-MP 5.0

97   (He et al., 2023).

98

99   Converting FORTRAN code into C# is not straightforward due to significant syntax differences

100   between the two languages. The reconstruction of the model in C# follows an object-oriented design.

101   While FORTRAN is traditionally a function-based language, the core Noah-MP module's functions,

102   subroutines, and state variables are encapsulated as members within a C# class named GridCell (**Fig.**

103   **1(a)**). This class represents all Noah-MP behaviors within a grid box. The variable names, function

104   definitions, data structures, and execution logic have been kept largely consistent with the original

105   FORTRAN code, ensuring user-friendliness for those familiar with Noah-MP. To handle the execution

106   on multiple grid boxes, another C# class named Driver is employed. This class manages tasks such as

107   initializing model variables, creating multiple grid boxes, reading/writing files, and controlling the

108   execution of the model.

109

110   Throughout the translation process, a key focus was addressing operations on FORTRAN arrays (**Fig.**

111   **1(b)**), crucial for representing the state of soil and snow layers in Noah-MP. Unlike C#, FORTRAN

112   allows arrays to have user-specified index ranges (e.g., index values from -3 to 4). However, in C#, the

113   first index of all arrays invariably starts from 0. To streamline the translation, we designed a wrapping

114   class of C# arrays, named FortArray, to mimic FORTRAN arrays. The wrapped inner array data in

115   FortArray adheres to standard C# conventions, accepting 0 as the inner index of the first element. Yet,

116   externally, the class allow access to the array values through extra indices by providing methods for

117   index translation from outer indices (FORTRAN style) to inner indices (C# style):

118      $I_{in} = I_{ex} - I_{start}$ (1)

119   Where I_{in}, I_{ex} and I_{start} represent the inner index, the outer index and the first outer index. The inner index

120   corresponds to the standard C# arrays, while the outer index corresponds to the FORTRAN arrays. For

121   instance, if a FORTRAN array of 8 elements has an index range from -3 to 4, it will be translated into a

122   FortArray that has a standard inner array of 8 elements, accompanied by two arguments representing the

123   starting FORTRAN index (-3) and the ending FORTRAN index (4), but the range of its inner indices

124   remain 0~7. This array translation technique ensures that all the original execution logic in Noah-MP is

125   seamlessly preserved in NMH-CS.

126

127   The model also supports parallel execution, implemented through the native parallel functionality of the

128   C# language. The technique can efficiently allocate computational tasks over the grid boxes to different

129   threads which can be executed by separate CPU cores. For instance, if a grid domain requires the

130   execution over 2400 grid boxes, and the tasks are assigned to 8 threads, each thread is responsible for

131   the calculations on approximately 300 grid boxes. It's crucial to note that if the number of specified

132   threads exceeds the number of CPU cores, several threads should be executed by the same CPU core.

133   Therefore, specifying more threads than the available CPU cores does not contribute to an overall

134   improvement.

135
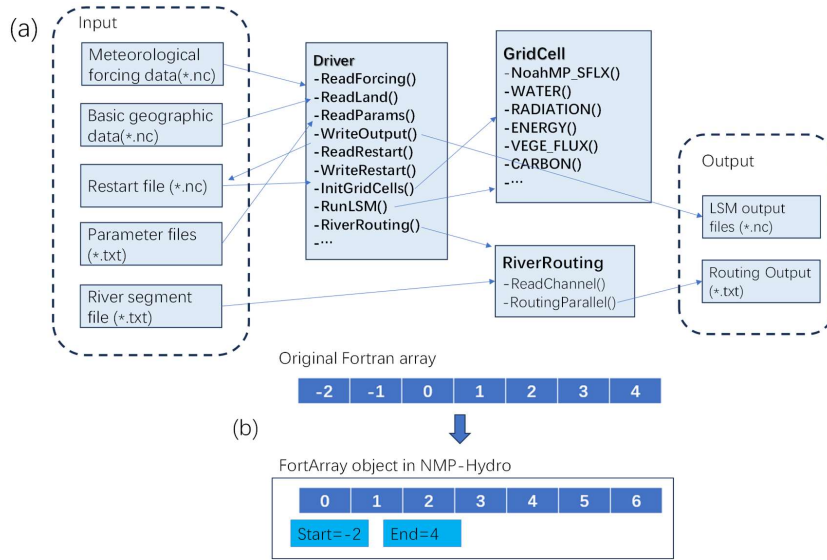
Figure 1. The architectural diagram of NMH-CS (a) and the conversion of FORTRAN arrays to C#
arrays (b). NMP-Hydro is a reconstructed replica of the version of Noah-MP that is coupled in WRF-
Hydro 3.0.

3.2 Coupling with a parallel river routing module

The Noah-MP land surface model can produce column outputs of runoff, but cannot simulate the
horizontal movement of water. In order to simulat~~cing~~ the surface movement of runoff in the river
channels, we integrated a parallel river routing module, which is based on the Muskingum method for
vectorized channel networks. The module is described in a previous study (Liu et al., 2023). This module
is not the previous RAPID model that was coupled in WRF-Hydro (Lin et al., 2018). This parallel river
routing module, implemented using C#, incorporates our unique techniques.

The first technique is an array-based sequential processing method for Muskingum routing. Muskingum-
Cunge equation (Cunge, 1969) with lateral inflow considered is

$$Q_{e,t+1} = C_0 * Q_{s,t} + C_1 * Q_{s,t+1} + C_2 * Q_{e,t} + C_3 * Q_{lat,t+1} \qquad (2)$$

Where

$$C_0 = \frac{kx + 0.5\Delta t}{k(1-x) + 0.5\Delta t}, \quad C_1 = \frac{-kx + 0.5\Delta t}{k(1-x) + 0.5\Delta t}, \quad C_2 = 1 - C_0 - C_1, \quad C_3 = \frac{\Delta t}{k(1-x) + 0.5\Delta t}$$

Here, Q represents the channel streamflow (m^3/s), which can be considered as a function of time and
position; s is the start point of a channel segment/node; e denotes the end point of the channel segment,
both of them are used as subscriptions for different spatial positions; t denotes the start of the period or
inflow, $t+1$ denotes the end of the period or outflow; Both t and $t+1$ are used as subscriptions for
position. The subscription 'lat' represents the lateral streamflow(runoff) from current river catchment.

Two parameters of the Muskingum-Cunge method are k and x. k is the travel time of a flow wave with
celerity c_k through a channel segment of length L, thus $k=L/c_k$.   Parameter x can be estimated by

159
$$x = \frac{1}{2}\left(1 - \frac{q}{S_o c_k L}\right) \qquad (3)$$

160 Where q represents unit width streamflow, S_o is the channel bed slope.

161 The lateral inflow of each river segment is the runoff simulated by column Noah-MP LSM in NMH-CS,
162 which is expressed as
163

$$Q_{\text{lat},t} = R_{c,t} A_s \qquad (4)$$

164
165 Where $Q_{\text{lat},t}$ is the lateral inflow at time t, R_c is the runoff value at the given grid box, A_s is the local
166 catchment area of current channel segment.

167
168 The form of Eq.(2) implies that the river routing calculation can be completed from any upstream river
169 segment to its downstream segment. At the time t+1, all the outflows ($Q_{e,\,t+1}$) of multiple upstream
170 segments will be summed up as the inflow ($Q_{s,\,t+1}$) of current segment. Although a common river network
171 is a tree-like structure, it can be represented as a sequential array, where any upstream river segment is
172 stored near the array head (with zero index), while its downstream river segment is stored near the array's
173 tail (with large array index). Therefore, the Muskingum routing can be calculated over the river segment
174 array in a unidirectional processing way (please see Fig.1 in Liu et al. (2023)).

175 The second technique is the straightforward equal-sized domain decomposition method to conduct
176 parallel calculation: just allocating the river segments into equal-sized blocks. Within each block, the
177 Muskingum routing can be executed separately by a single CPU core. This treatment is based on that in
178 any block, most segments have upstream segments within the same block, and only a small fraction of
179 the segments have upstream segments in other blocks. Therefore, all river segments that receive inflows
180 from other blocks (referred to as 'cross-block segments') need to be identified. These cross-block
181 segments should be executed by the primary core, after the multi-domain parallel execution is completed.
182
183 The third technique is a specific sorting approach for river segments used in domain decomposition. It
184 has been proven that a depth-first traverse of the river segments is more suitable for the parallel execution
185 of the Muskingum method, compared to a width-first traverse, due to less cross-block segments in the
186 blocks.
187
188 This module requires two additional inputs files, a river segment list file named 'ChannelOrder.txt' and
189 a 'namelist.txt' file. The latter file is used to set parameters and the length of time step. Each river segment
190 in the list file presents following information: its own index, the index of its next downstream river
191 segment, the row number and the column number of the grid box (in Noah-MP's running domain)
192 providing runoff input to the current segment, the length (m) of the current river segment, the two
193 parameter values (K and X) of the Muskingum method, the area of the catchment of the current segment.
194
195 The river segment list can be derived from both gridded river network or vectorized river network. The
196 resolution of the river routing is determined by the original river network from which river segments is
197 derived. Therefore, the choice of using vector river network or gridded river network and the selection
198 of spatial resolution are completely determined by the users. The length of the temporal step of the river
199 routing is required to be multiple times shorter than the time step for running the Noah-MP, and can also
200 be designated by the users. For example, the time step of routing is set to 600s, while the time step for
201 Noah-MP LSM is usually set to 3 hours.

202

203 This approach's primary advantage lies in its ability to simply decompose any river network into multiple
204 domains with an equal number of river segments. Achieved by evenly dividing the river segment list into
205 any number of blocks, this innovation capitalizes on the inherent tree-like structure present in most river
206 networks. Importantly, it does not necessitate consideration of the topological conditions specific to a
207 given network, as required in studies such as Mizukami et al. (2021) or David et al. (2015). This design
208 allows parallel execution of river routing on modern personal computers equipped with multi-CPU cores.

209

210 The integration of the river routing module with the Noah-MP LSM involves assigning lateral inflows
211 from the LSM-simulated total runoff to the river routing model. In the present NMH-CS configuration,
212 we utilize a catchment centroid-based coupling interface (David et al., 2015). This method designates
213 the LSM grid cell containing the catchment centroid (referred to as the "centroid cell") as the location
214 for a river reach to receive lateral inflows. At a specific temporal step, the computed contributing runoff
215 discharge Q_{lat} (unit: m³/s) is determined by the following expression:

216 $$Q_{lat} = R(nx, ny) \times F \times 1000 \qquad\qquad (5)$$

217 where $R(nx, ny)$ is the runoff (mm, surface + subsurface) simulated by the LSM during the time step,
218 F is the catchment area (km²) contributing water to the current river segment.

219

220 Alternatively, employing weighted assignments from different grid boxes, akin to the method utilized in
221 (Lin et al., 2018), is also a valid approach. However, this method requires the generation of weights from
222 multiple grid boxes. Given the rough resolution of the meteorological datasets, each grid box can
223 encompass the catchment areas of multiple river segments, the coupling approach using area weighting
224 is unlikely to yield substantial improvements for most river segments.

225 **3.3 Code Debugging Process**

226 To eliminate any potential code errors resulting from incorrect translation, we conducted a thorough
227 checking of the code by performing model execution benchmark tests on single-column running on
228 specific grid boxes. Here, In the large domain (the same domain described in section 4.1), each time the
229 grid box for single-column execution is arbitrarily selected. Such debugging tests were carried out in two
230 approaches. The first approach was carrying out a meticulous step-by-step debugging by examining the
231 printed values of many variables (including many local variables in the code) in WRF-Hydro 3.0. This
232 process was also repeated by switching each option of multiple physical parameterization schemes. The
233 grid box for the single-column debugging was also switched several times. Such debugging has been
234 conducted numerous times and has effectively eliminated any code errors arising from inaccurate
235 translation. Although meteorological driving data for the debugging simulation is prepared for the period
236 between 2000 and 2016, such debugging tests are only feasible for a limited number of temporal steps
237 for a grid-box execution. It is also impossible to conduct debugging on the entire domain.
238 The second approach is an artificial code checking process. Considering that the stepwise debugging
239 through years-long simulations is impractical, we checked the NMH-CS's code by comparing with the
240 original FORTRAN code for many times. Through this checking, many code inconsistences were
241 identified and corrected.

242

4. Testing of NMH-CS

4.1 Application area and data

4.1.1 Application area

The Yellow River Basin in Northern China is used as a test area of NMH-CS. The gridded domain, as illustrated in **Fig.2-3**, encompasses the entirety of the Yellow River Basin (YRB) and most of North China, comprising of 350 columns and 170 rows, with a resolution of 6 km in Lambert conformal conic projection coordinates. Geophysical data essential for the domain, including digital elevation, land use and land cover, and green vegetation fraction, were extracted from the WRF/WPS 3.5 input database.
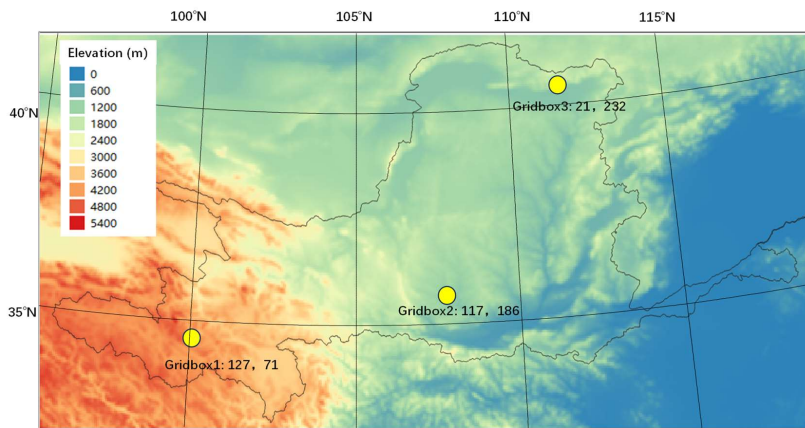
Figure 2. The terrain map of the simulation domain and the three grid boxes for comparison of state variable time series. The three grid boxes for extracting state variables to compare are represented by yellow dots, marked with grid box code, the row number and the column rows.

For the river routing simulation, the digital river network of the Yellow River was obtained from the HydroSHEDS dataset (version 1) (http://hydrosheds.cr.usgs.gov/). HydroSHEDS was derived from gridded digital elevation data with a resolution of 15 arc-seconds. Given the substantial human intervention and the intricate nature of reproducing observed daily or hourly water discharge, uniform values were assigned to all river segments for the river routing parameters (specifically, the wave celerity (c_k) and another parameter (x) describing the river channel condition, as detailed in David et al. (2013). No precise calibration is required here, as monthly or annual river discharge remains unaffected by changes in routing parameters.

The Yellow River basin experiences significant human impacts, including irrigation, industrial water usage, and groundwater extraction. Major artificial reservoirs and numerous smaller reservoirs regulate the river's discharge, serving as the primary water resource during the dry season. However, such extensive human interference presents substantial challenges in accurately modeling river discharge. Comparatively, the river discharge upstream of the Lanzhou (In Zone 1 as shown Fig.3) hydrological station contributes over half of the entire YRB's total discharge, and is relatively less impacted by dams, enabling us to test the model's performance.
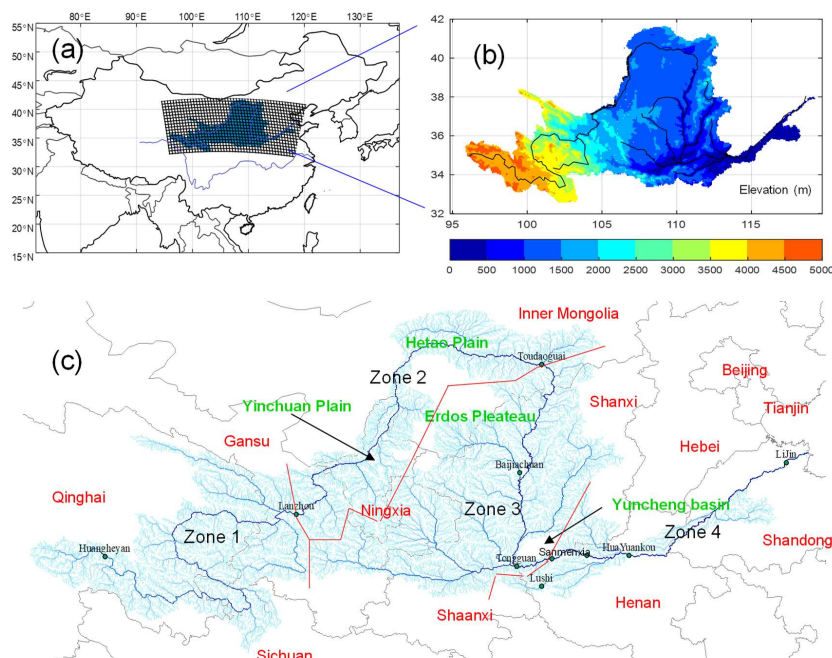
Figure 3. The grid domain covering the Yellow River Basin and the North China area: (a) Geographical location within China; (b) Elevations; (c) Vector River networks utilized for river routing modeling (extracted from the HydroSHEDS dataset). The delineation of the boundaries between distinct zones controlled by four gauging stations (Lanzhou, Toudaoguai, Sanmenxia, Lijin) is represented by red lines.

4.1.2 Meteorological dataset and river discharge data

To drive the two models (NMH-CS and WRF-Hydro), the same 3-hourly and 6-km grided meteorological forcing dataset comprised of shortwave and longwave downward radiation, wind velocity, air temperature, relative humidity, air pressure at the surface, and precipitation rate was acquired. The benchmark dataset was clipped and regrided (bilinear interpolation) from the 1.0°×1.0° GLDAS-1 land surface product (Gan et al., 2019; Rodell et al., 2004), for the period 2000-2016. Given the limited availability of observational river discharge data between 2001 and 2016, the extracted data pertains to this period, and additional data between 1996 and 2000 was also extracted for the model's spinning-up. In previous research, the spinning-up of Noah-MP requires 50 years (Wu et al., 2021) or more than one hundred years (Zheng et al., 2019) to achieve an equilibrium state. However, in this study, the spin-up process was conducted in two steps. In the first step, the period from 1996 to 2016 was run three times to generate a 'restart file' for a 63-year spinning-up, utilizing the initial PS combination. In the second step, starting from this initial combination, new schemes were adopted, and the 'restart file' obtained from the initial scheme combination was used to initiate the formal experiments covering the period from 1996 to 2016.

The dataset of Natural River Discharge (RND) reconstructed by the Yellow River Conservancy

293   Commission of the Ministry of Water Resources was gathered to assess the model output. Annual natural

294   discharges from the monitoring station of Lanzhou were collected for the period from 2001 to 2016.

295   **4.2 Running speed**

296   Compared to other differences between the two models, running speed is the least important factor to

297   consider. Considering that NMH-CS and WRF-Hydro run on different platforms (Windows or Linux)

298   and machines, it is also difficult to achieve a comparative evaluation of running speed. Actually, the

299   comparison of running speed depends on the programming language used. In theory, FORTRAN and C

300   programs can run faster than C# programs because FORTRAN and C are relatively low-level languages

301   compared to any modern object-oriented language. However, as a language that can run in native

302   machine code, C# is not slow. This means that there won't be a large difference in running speed between

303   C# and FORTRAN. There are few authoritative publications on the running speed of these two languages,

304   but there have been many documents on benchmark testing on the internet. When considering parallel

305   execution, comparing the running speed of the two models also become more unnecessary. NMH-CS can

306   run in parallel mode on personal computers, while WRF-Hydro does not have this functionality. On the

307   other hand, WRF-Hydro can run in parallel mode in the Message Passing Interface (MPI) environment

308   of high-performance computers, while NMH-CS does not support MPI.

309   We tested the execution time of NMH-CS by setting different numbers of C# parallel threads. The

310   computer used for the testing is a common laptop with 6 CPU cores. The results indicate that for the

311   execution of the entire domain, as the number of threads increases from 1 to 6, the average time consumed

312   per time step is 1576ms, 977ms, 801ms, 711ms, 679ms, and 672ms, respectively. When the number of

313   threads is set to 1, the time spent is slightly greater than the execution time in the non-parallel mode

314   (1461ms). It is worth noting that the time spent is not linearly related to the number of parallel threads,

315   which can be explained by various reasons. One is that some tasks are not actually executed in parallel

316   mode, such as reading meteorological input files. Another reason is that not all threads in NMH-CS are

317   fully processed by the CPU cores, as there are many other tasks in the entire Windows environment that

318   have to be processed simultaneously by the CPU cores.

319   **4.3 Comparing the outputs of NMH-CS and WRF-Hydro**

320   It is noteworthy that there are numerous parameterization scheme combinations for Noah-MP, which

321   makes it unfeasible to compare the results generated under all scheme combinations. Therefore, the

322   output of NMH-CS and WRF-Hydro was compared only with the default parameterization scheme

323   combination, based on the exact same meteorological dataset. The comparison was conducted in two

324   ways. The first comparison is that of the spatial maps of multiple variables (Table 2) for a specific year

325   or day. For each state variable, such as SFCRNOFF, the maps of state variables simulated by NMH-CS

326   and WRF-Hydro are presented. The difference (Δ) between the values of the same variables simulated

327   by the two 'Noah-MP models' is calculated as

328    $\Delta = V_{\text{NMH-CS}} - V_{\text{WRF-Hydro}}$ (6)

329   Where $V_{\text{NMH-CS}}$ and $V_{\text{WRF-Hydro}}$ are the state variable simulated by the two Noah-MP models, respectively.

330   For certain variables, such as SFCRNOFF, UGDRNOFF, ECAN and ETRAN, the percent relative

331   differences were also calculated as follows:

332    $\delta = 100 \cdot \Delta / V_{\text{WRF-Hydro}}$ (7)

333   The second method is to compare the temporal variations of state variables at specific grid boxes. In this

case, only three grid boxes (Fig. 2) were selected to extract the state variable time series. The selection of these grid points is an arbitrary decision made by roughly considering different climate zones, without other strict consideration. Gridbox1 is selected from the Qinghai Plateau region, corresponding to the source region of the Yellow River. Gridbox2 corresponds to a location of Inner Mongolia and the north of Loess Plateau. Gridbox3 is in a hilly area of the Wei River Basin (a major part of the Yellow River Basin). In fact, during this study, other grid points also have been casually tested, but the results are mostly similar to the above mentioned 3 grid boxes. and will not be presented in the paper.

Table 2 The state variables simulated by NMH-CS and WRF-Hydro, which is verified by generating maps

Variable name	description	unit
SFCRNOFF	Accumulated Surface runoff	mm
UGDRNOFF	Accumulated ground runoff	mm
ECAN	Evaporation from canopy	mm
ETRAN	Vegetation transpiration	mm
TV	Vegetation temperature	K
TG	Ground temperature	K
SOILT	The temperature for soil layers	K
SOILW (or SH2O)	The volumetric content of moisture in soil layers	$m^3 \cdot m^{-3}$
SNOWH	The total depth of snow layer	m
SNEQV	Snow water equivalent	$kg \cdot m^{-2}$
EAH	Canopy air vapor pressure	Pa
EVG	Ground evaporation heat	$W \cdot m^{-2}$
CHV	Exchange coefficient vegetated	$m \cdot s^{-1}$
CHLEAF	leaf exchange coefficient	--
TR	Transpiration heat	$W \cdot m^{-2}$
EVB	Evaporation heat to atmosphere bare	$W \cdot m^{-2}$
FIRA	Total net long-wave radiation to atmosphere	$W \cdot m^{-2}$
TRAD	Surface radiative temperature	K
ALBEDO	Surface albedo	--

4.3.1 Maps of state variables

To test whether NMH-CS can produce the corresponding outputs of the original WRF-Hydro (Fortran-version Noah-MP), many state variables (Table 2) from multiple time slices have been checked by drawing maps. Only four slices (10 June 2000, 10 June 2001, 10 June 2004, and 10 June 2008) were arbitrarily selected here without special consideration. Only some maps of these state variables at certain time slices are presented in both the paper and the supplementary information. The maps for all the sate variables in Table 2 reflect high consistence between NMH-CS and WRF-Hydro, with only the maps for fourtwo representative variables (SFCRNOFF, UGDRNOFF, —and TV and TG) are shown in **Fig.4 and Fig.5**.

As can be seen, there is visually little difference in the spatial patterns of the results. Similarly, no discernable visual difference is also apparent for the maps of other variables. However, the relative

356 difference of annual surface runoff and annual underground runoff is significantly large at some areas
357 (generally in high-elevation regions), where NMH-CS underestimated/overestimated those values above
358 10% (**Fig.4**). These regions with large relative differences of underground runoff actually are in small
359 absolute differences, primarily because the annual total groundwater runoff in these areas is inherently
360 low (<50 mm). This discrepancy is likely attributable to floating-point arithmetic errors, but the
361 possibility of other contributing factors cannot be ruled out.
362 –For most of the domain, the difference in TV is smaller than 0.2 ℃, but in some sporadically districted
363 locations, the TV's difference can be larger than 2 ℃ (**Fig.5**). The comparison of TG has the similar
364 effects, but the difference is more significant than that of TV. The similar high consistency effects are
365 also reflected by other state variables, including soil temperature, soil water content, snow water
366 equivalent (**Fig.S2-S4** in supplementary information). The differences in these state variables between
367 the two models are generally small, except some large ones sporadically distributed in the high-latitude
368 areas.

Formatted: Font color: Auto

369

370
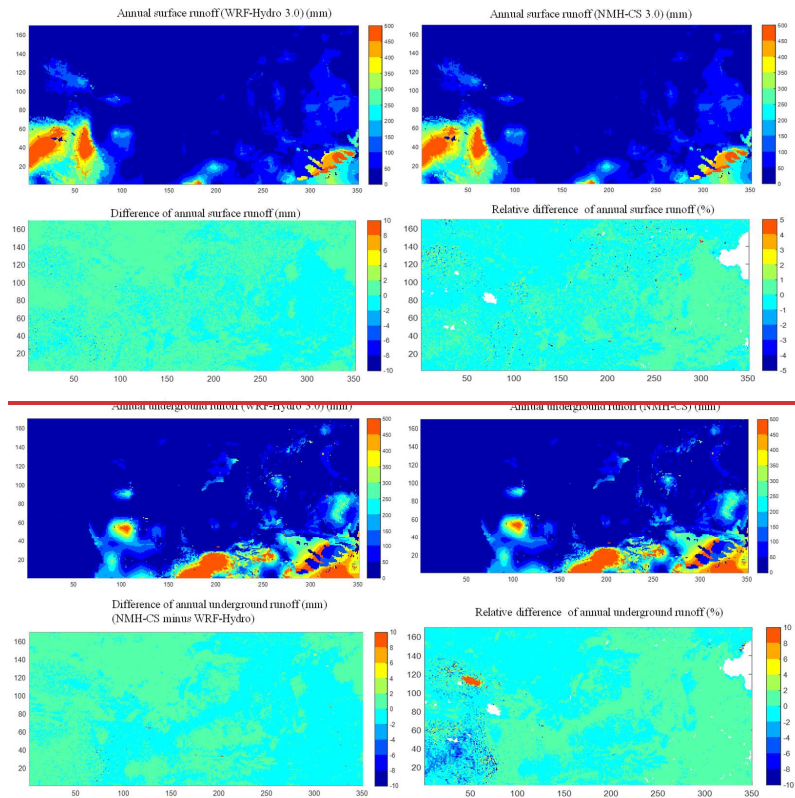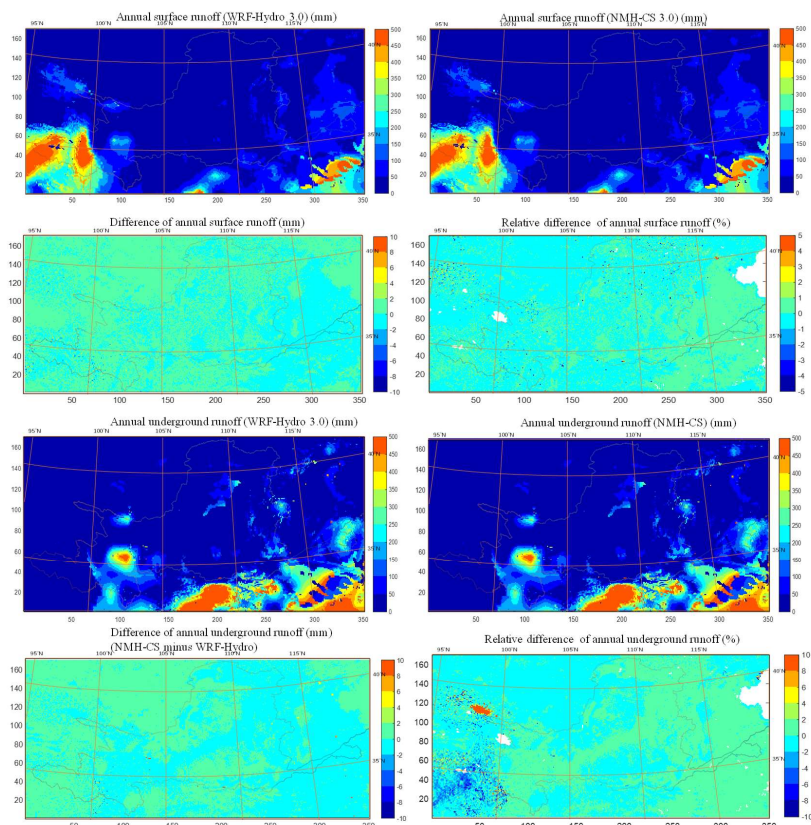
Figure 4. Maps of annual total values, differences, and relative differences of SFCRNOFF (surface runoff, mm) and UGDRNOFF (underground runoff, mm) simulated by WRF-Hydro3.0 and NMH-CS 3.0, for the year 2005. The labels for horizontal axis and vertical axis are row numbers and column numbers of the grid domain respectively.

375

376

377
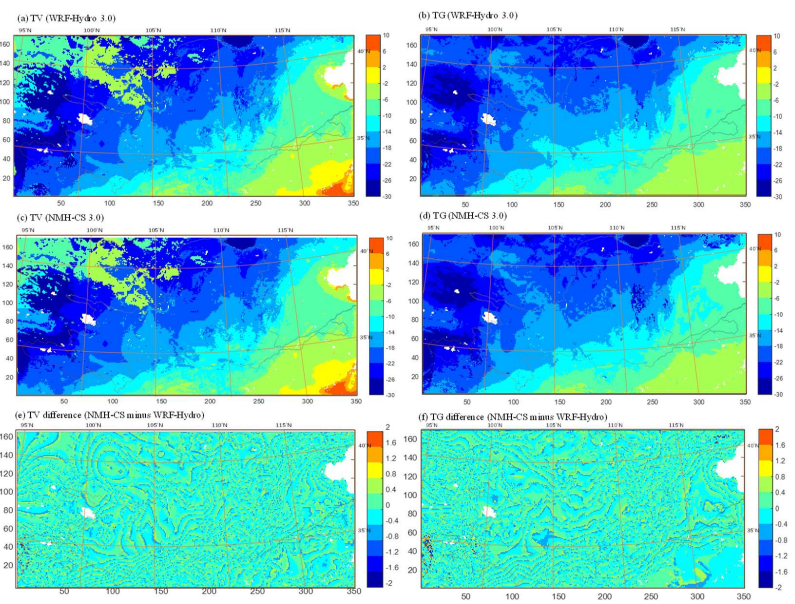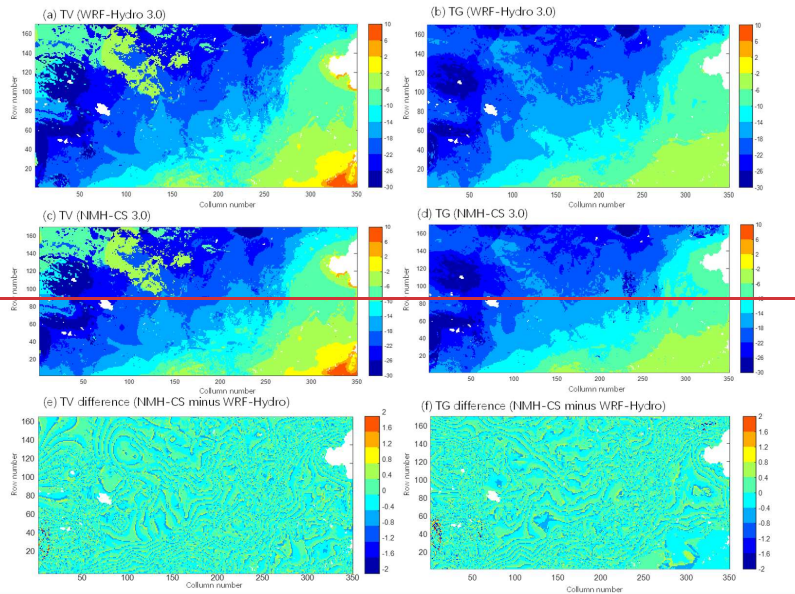
Figure 5: Similar to Fig.4, but the maps for Maps of TV (vegetation temperature, ℃) and TG (ground temperature, ℃), simulated by WRF-Hydro3.0 and NMH-CS 3.0, for the day Jan. 1st, 2008.

380

381 **4.3.2 Temporal variations of state variables**
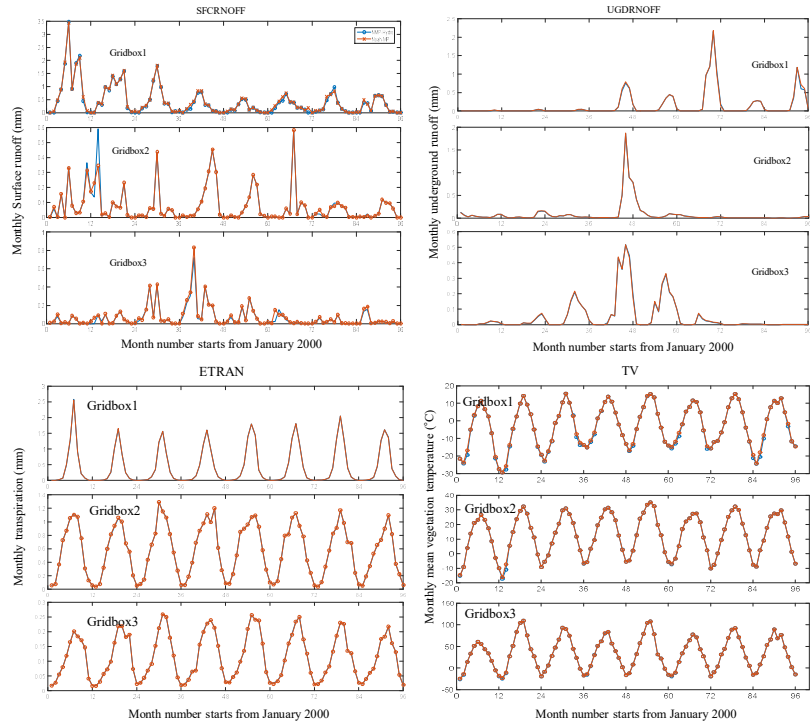
382

383 **Figure 6:** Monthly surface runoff (SFCRNOFF in mm), underground runoff(UGDRNOFF in mm),
384 transpiration (ETRAN in mm) and vegetation temperature (TV in ℃) simulated by WRF-
385 Hydro3.0(~~Noah-MP,~~ blue) and NMH-CS (red) at the three grid boxes, 2000-2007.

386

387 The outputs at the three representative grid boxes (as shown in **Fig.2**) indicate that the two models
388 produced consistent temporal changes (**Fig.6, Fig.S5 and Fig.S6**). For certain variables, for example,
389 SFCRNOFF, TV and TG (other variables as well), occasionally, some significant differences were
390 found in certain months for Gridbox2. It must be such occasionally happened differences that caused
391 the spatial disparity as shown in **Fig.4-5**. We checked the disparity at certain grid boxes on the 3-hourly
392 values and found that the differences also happen sporadically (**Fig.7**). Almost all the disparities occur
393 during the cold months (November, December, January, and February). However, it is worth noting that
394 mostly the simulated state variables in these months show no difference. Considering such mismatch
395 usually happens in cold months and high-elevation regions, it may be caused by the different
396 calculation accuracy for the processes of snow or frozen soil. For the three representative grid boxes,
397 no significant differences were identified for certain variables, including many variables like TR, EAH,
398 TV, ETRAN, UGDRNOFF (no plots for these variables will be presented in the paper).
399 By comparing and analyzing the printed state variables (in 3-hourly timesteps) in WRF-Hydro and the
400 NMH-CS, we found the major inconsistencies occur in the module of snow water (named

‘SNOWWATER’ in the code). From **Fig.7**, three major inconsistencies simulated between the two models occur usually simultaneously in the multiple state variables. These three cases demonstrates that almost all the major inconsistencies in multiple variables are caused by the minor inconsistencies in SNOWH (the state variable to indicate the depth of snow). The logic of snow process in Noah-MP is coded as when SNOWH is below 0.025m, the ISNOW (a state variable to indicate whether snow a layer exists) is set to zero (no snow layer), otherwise, is set to 1 (having a snow layer). Therefore, if SNOWH simulated by NMH-CS is close to 0.025, a small floating-point error may trigger a division between having a snow layer and no snow. Due to the different physical effects of radiation balance between snow layers and the ground, the distinction between having a snow layer and no snow layer will further lead to significant inconsistencies in snow depth (SNOWH), snow water equivalent (SNEQV), soil water (SOILW), vegetation temperature (TV), and ground temperature (TG). Once an inconsistency occurs, it will persist for a period of time. It is highly probable that the minor differences in SNOWH is caused by accumulation of floating-point error, because for most of the times the differences are very small except those during the inconsistent periods. This explanation may account for the inconsistencies observed in the time series in Fig. 7 and the sporadically distributed discrepancies in high-latitude regions depicted in Fig. 4.

3-hourly timestep number since Jan. 1st, 2000 0:00
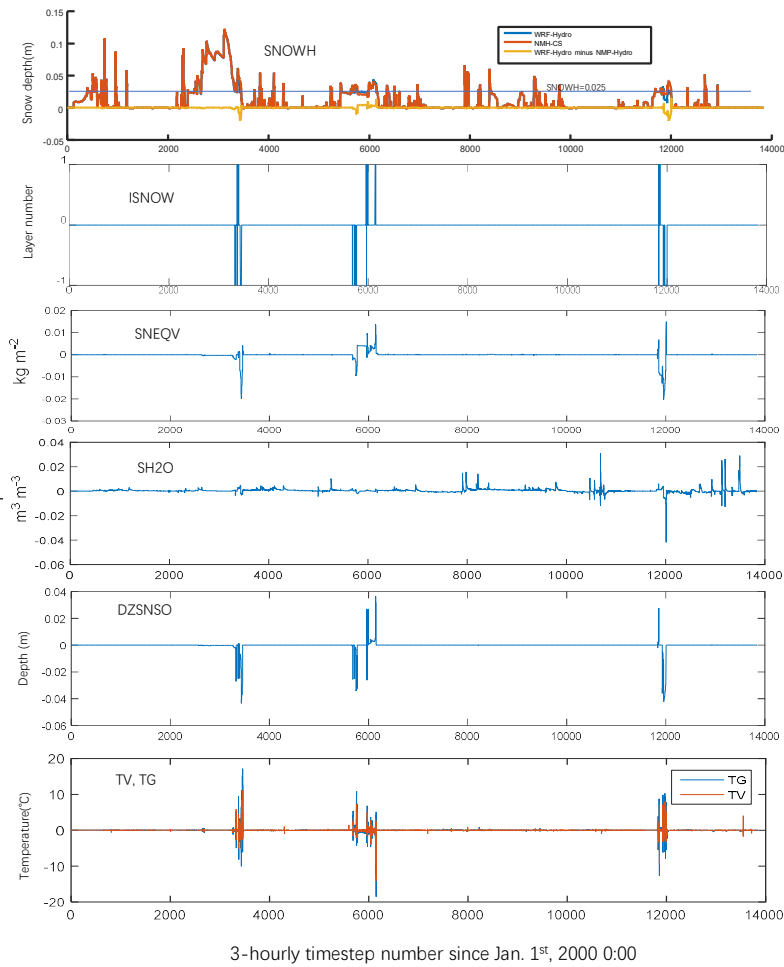
Figure 7: The differences (NMH-CS minus WRF-Hydro) between the three-hourly variables simulated by NMH-CS and those simulated by WRF-Hydro. SNOWH: snow depth (m); ISNOW: Number of snow layers, count; SNEQV: Snow water equivalent (kg·m^{-2}); SH2O: soil liquid water content (m^3·m^{-3}), equivalent to SOILW; DZSNSO: snow/soil layer depth (m). These variable names are those used in the programming code. The occurring of the three inconsistencies correspond to the short periods: March 4, 2001, January 15, 2002 to February 8, 2002, and January 22, 2004 to February 9, 2004.

The daily time series from multiple grid boxes (including the three in Fig.2) were extracted and compared between NMH-CS and WRF-Hydro. Similar effects were obtained for the grid boxes, but only the results for Gridbox3 are presented as representative in **Fig.8**. It is evident that EDIR, SFCRNOFF, soil water content (SOILW) and TV exhibit small discrepancies, whereas TG demonstrate large disparities. The daily samples for soil temperature, soil water content, snow depth and snow water equivalent are presented in **Fig.S1, Fig.S5 and Fig.S6** (supplementary material). The comparisons about soil layers

432 reflect that the soil temperature has relatively large inconsistencies, which should also be explained by
433 the different division of snow layers that is caused by error when SNOWH approaches 0.025m.
434
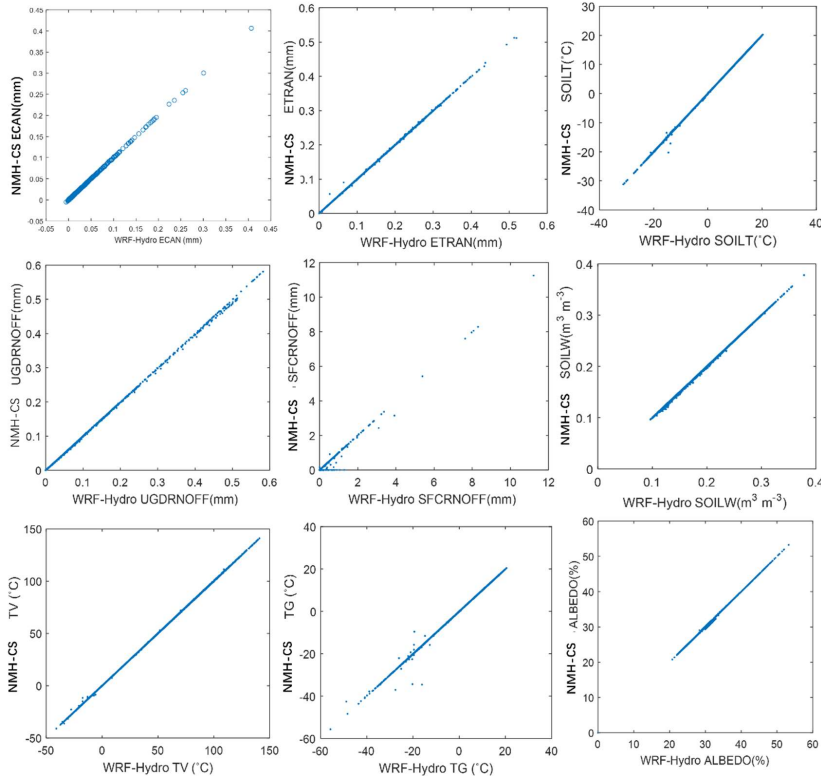
436 **Figure 8.** Daily state variables simulated by NMH-CS versus by WRF-Hydro at Gridbox3. Due to the
437 high consistency for most of the values, statistical evaluation metrics such as correlation coefficients or
438 relative biases will not be presented in the paper.
439
440

441 **4.4 Streamflow discharges for the Yellow River by NMH-CS**

442 **4.4.1 Experimental design of Noah-MP simulation**

443 Here, we present the numerical outputs of NMH-CS on the streamflow discharges over the Yellow
444 River, with various parameterization schemes used. To verify whether the various parameterization
445 schemes (PSs) of NMH-CS can produce reasonable discharge for the Yellow River catchment area,
446 this study conducted 17 Noah-MP simulations using different PS combinations. Given the challenge
447 of determining the relative importance of each parameterization and the impracticality of including
448 all possible combinations, we adopted a strategic approach. A fixed PS combination was established
449 as a foundation, and alterations were made to one parameterization's scheme at a time (refer to **Table**

450 **3**).

451 In addition to our selected parameterizations, we considered commonly used PS combinations,
452 including the 'default' combination proposed by Noah-MP developers. Sensitivity analysis was
453 conducted by analyzing the differences or variations among these incomplete PS combinations. It
454 is important to note that the chosen PS combinations represent only a subset of all possible
455 combinations, and the assumed sensitivities based on this subset are considered indicative of overall
456 sensitivities based on the complete set of combinations.

457 The PS combinations are represented by codes consisting of sequential digital numbers. For instance,
458 the default combination is denoted as '11131-1132-111', where each number signifies a scheme
459 option. The initial experiment, arbitrarily set as the PS combination of '11131-2222-121', served as
460 the foundation for subsequent experiments. Fifteen experiments (refer to Table 2) were then
461 conducted by modifying one option at a time from the initial experiment.

462 These experiments are categorized into multiple groups, with the initial experiment '11131-2222-
463 121' being employed in multiple groups:

464 Runoff scheme group (four experiments, switching between: 1. SIMGM, 2. SIMTOP, 3. Schaake96,
465 4. BATS);

466 Vegetation scheme group (five experiments, switching between the first option and the fifth option,
467 see Table 1);

468 β-factor option group (three experiments, switching between Noah, CLM, and SSiB);

469 Radiation transfer option group (three experiments, switching between three options);

470 Group for the scheme of the lower boundary of soil temperature (six experiments);

471 Group for stomatal conductance scheme (two experiments, switching between two options).

472

473 **Table 3.** Experiments conducted in this study

Number	PS combination code	Abbreviated code	Description
1	11131-2222-121	11131 or 11131-222 or 11131*121	The control experiment
2	11111-2222-121	11111	Experiments with RUN
3	11121-2222-121	11121	
4	11141-2222-121	11141	
5	21131-2222-121	21131 or 21131*121	Experiments with DVEG
6	31131-2222-121	31131	
7	41131-2222-121	41131	
8	51131-2222-121	51131 or 51131*121	
9	11231-2222-121	11231	Experiments with BTR
10	11331-2222-121	11331	
11	11131-2212-121	11131-221	Experiments with RAD
12	11131-2232-121	11131-223	
13	12131-2222-121	12131	Experiments with CRS
14	11131-1132-111	'default'	The default PS combination proposed by Noah-MP

			developers
15	11131-2222-111	11131*111	Experiments with TBOT
16	21131-2222-111	21131*111	
17	51131-2222-111	51131*111	

474

4.4.2 Simulated streamflow under various parameterization schemes

476 The Taylor diagrams (Taylor, 2001) are used to evaluate the different PS on the river discharge at the
477 Lanzhou station. Taylor diagram provides a graphical representation of a model's simulation performance,
478 encompassing three key indices: correlation coefficient (R), root-mean-square error (RMSE), and
479 standard deviation (SD).
480 The streamflow discharges were produced by coupling the NMH-CS with the parallel river routing model.
481 A preliminary comparison on the various scheme combinations is presented in **Table 4**. The monthly
482 performance is summarized in Table 4 based on the comparison of the different PSs as shown in **Fig. 9**.
483 It can be observed that for the majority of parameterizations, the discharges in winter are not sensitive to
484 the schemes, this is to be expected, given the minimal runoff during this season. The simulated summer
485 discharges exhibit notable degree of sensitivity with regard to the various parametrization schemes. In
486 relation to the runoff parametrization, the results obtained through the utilization of the SIGGM scheme
487 led to overestimation during the winter season and underestimation during summer, signifying that
488 considering groundwater could enhance the simulation accuracy of the catchment modulation as opposed
489 to other schemes.
490 For the Lanzhou station, over 50% of experiments produced discharges with correlations larger than 0.9
491 (Fig.10). The PS combination '11141-2222-121' yielded the highest correlation, and '11131-2222-111'
492 showed the highest performance according to Taylor's score.
493
494

496
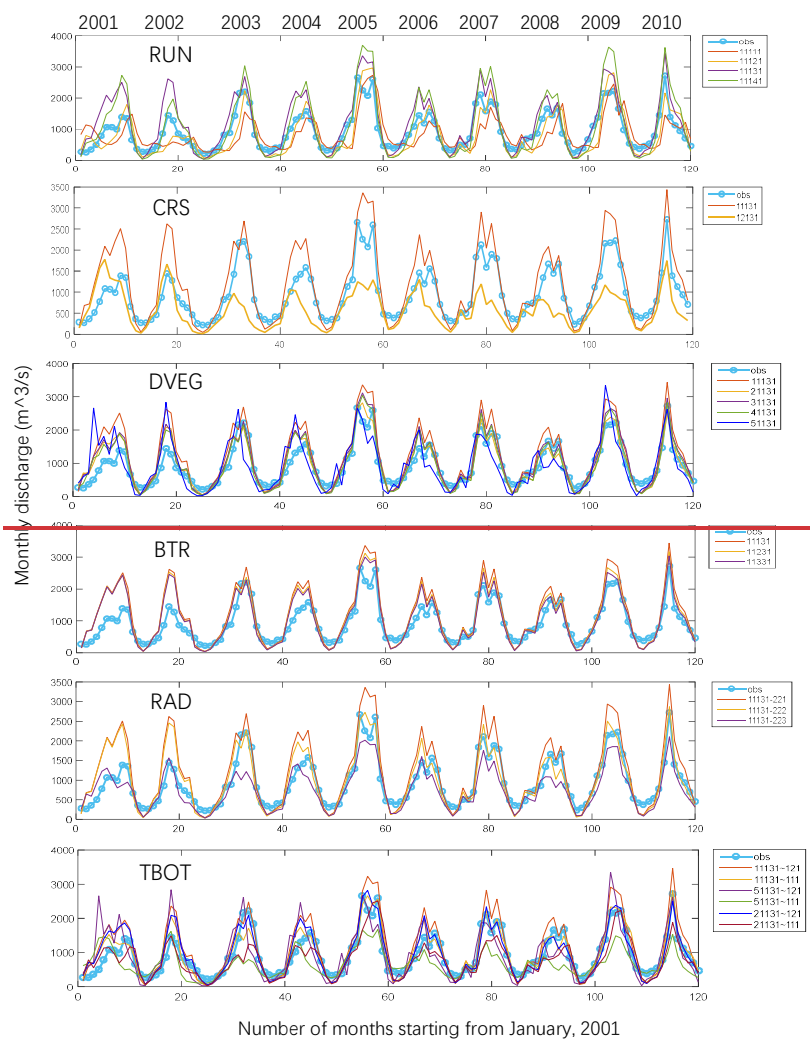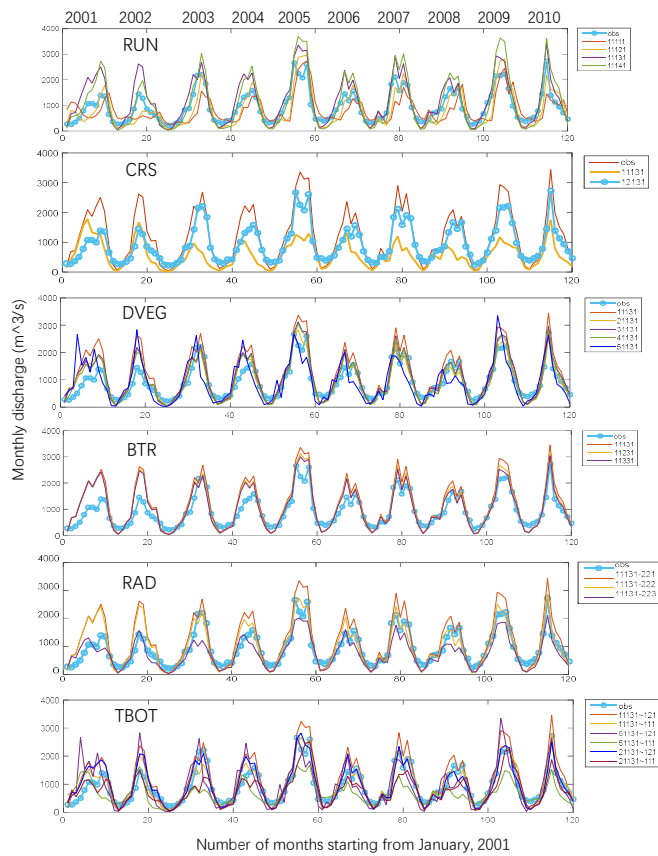
Figure 9: Simulated monthly river discharge (m³/s) for Lanzhou by NMH-CS. The first subplot displays the results simulated with varying RUN schemes while the other subplots follow a similar pattern. Reconstructed natural discharge is denoted as 'obs'.

500
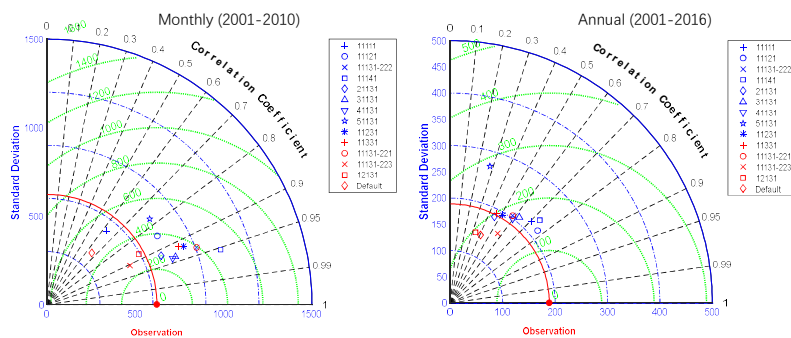
Figure 10: Taylor diagram for monthly and annual mean river discharge (m³/s) at the Lanzhou monitoring station

503
504 **Table 4**: Performance of various parameterization schemes on monthly discharge for Lanzhou station

	scheme	Winter	summer
RUN	1.SIGGM	Overestimation	underestimation
	2.SIMTOP	underestimation	Small overestimation
	3.Schaake96		Large overestimation
	4.BATS		The Largest overestimation
CRS	1. Ball-Berry	Small difference	Overestimation
	2. Jarvis		Underestimation
DVEG	1.Table LAI, read FVEG	No significant difference	The largest overestimation
	2.dynamical LAI and FVEG=f(LAI)		Mostly small overestimation
	3. table LAI, FVEG=f(LAI)		
	4 table LAI, FVEG=maximum		
	5.Dynamical LAI, maximum FVEG	Unstable overestimation and underestimation	
BTR	1.Noah	No significant difference	The largest overestimation
	2.CLM		The middle overestimation
	3.SSib		The smallest overestimation
RAD	1. gap=F(3D, cosz)	No significant difference	Large overestimation
	2. gap=0		Slight overestimation
	3. gap=1-FVEG		underestimation
TBOT	1. Zero flux	No significant difference	large
	2.Noah		small

505

5 Discussions

5.1 Major advantages of NMH-CS

508 The original intention of developing a Noah-MP model with the C# programming language was to
509 analyze and edit Noah-MP code in a more efficient way, as there are many modern and efficient tools
510 available for analyzing code written in C#, such as Microsoft Visual Studio, SharpDevelop
511 (https://github.com/icsharpcode/SharpDevelop). There are almost no comparable powerful tools for
512 analyzing FORTRAN code. This advantage is significant from the developers' perspective.
513 From the user's perspective, NMH-CS run on windows (although it should also run on other UNIX like
514 platforms after some specific configuration in the future), which is more favorable for many Windows
515 users around the world. On the windows system, in most cases, the NMH-CS software can be
516 distributed at multiple computers by simply copying it, unlike that in Unix-like systems, compiling of
517 the code is usually required.

5.3 Inconsistencies between the two models

519 As indicated by the previous analysis, the main inconsistency between the outputs of the two models
520 (WRF-Hydro and NMH-CS) was found to be related to the transition between the presence or absence

521 of snow layers. In Noah-MP, the existence of snow layers is determined by the depth of the snow
522 (represented by the variable SNOWH in the code). When the SNOWH value approaches the threshold
523 (0.025m), a small error will result in a division on the judgement whether a snow layer exists. This
524 inconsistent division will further lead to significant differences in other state variables. However, this
525 difference will not last long (as shown in Figure 3, up to 30-40 days). However, it is difficult to
526 determine whether the errors in SNOWH are caused by the accumulation of floating-point errors or
527 other errors.
528 There may be some other inconsistencies that has not been identified. Due to the complex nature of
529 Noah-MP, it is challenging to identify all the minor differences through the process of code checking
530 and debugging. Therefore, to ensure the results of two models to be completely consistent need a long-
531 term process. Discrepancies can be arisen from multiple factors, including floating-point calculation
532 errors, some inconsistent hardcoded parameter values (as local variables in certain modules), or
533 inconsistent programming code. The former two are reasonable and acceptable, whereas a coding
534 mismatch can cause unexpected outputs. From the scientific perspective, these minor differences
535 between NMH-CS and WRF Hydro are not very critical, as the model users are always modifying the
536 code during their research, and small changes in the code can lead to large different results. The
537 existence of differences does not always mean that NMH-CS is inferior to Noah-MP in WRF-Hydro
538 3.0.
539 In most cases, identifying discrepancies is only feasible during the debugging of the first 1-3 timesteps,
540 but not for tens to hundreds of subsequent iterations. It is not uncommon for errors to remain
541 undetected even after the execution of numerous time steps. In this study, given that no code
542 inconsistencies were found after multiple rounds of code checking, it is plausible that floating-point
543 errors related to SNOWH (or other related variables) play a major role in explaining the remaining
544 discrepancies.
545 Based on the debugging process, we also found that some variables such as TV and TG calculated by
546 the two models always have slight inconsistencies, but they are almost insignificant on a daily or
547 monthly scale. It is highly probable that such inconsistencies arise from the accumulated error caused
548 by the recursive calculation of energy transferring for vegetated and bare land.

6 Model code and technical documentation for NMH-CS

552 We archive, manage, and maintain the NMH-CS at https://github.com/lsucksis/NMH-CS for public
553 access. A technical description was provided at the same site. The original version of the model is also
554 provided at the website of Science Data Bank: https://doi.org/10.57760/sciencedb.16102.

7 Conclusions

556 This study presents the NMH-CS 3.0, which is a reconstructed land surface eco-hydrological model
557 based on Noah-MP. The model was developed by translating the FORTRAN code of Noah-MP (in
558 WRF-Hydro 3.0) into C# and also coupling it with a river routing model. The model has been designed
559 for parallel execution on Windows systems, thereby capitalizing on the multi-core CPUs that are now a
560 standard feature of personal computers. The NMH-CS code has been subjected to rigorous testing to

561   ensure that it produces results that are as consistent as possible with those of the original WRF-Hydro.

562   The code is based on the C# language, which facilitates greater user-friendliness and facilitates

563   modification and expansion.

564   The development of this software enabled the successful execution of 6-km high-resolution simulations

565   ~~encompassing a 6-km span within~~for a rectangular region covering the Yellow River Basin and North

566   China~~(YRB)~~. These simulations were conducted with a multitude of parameter scheme (PS)

567   combinations within the Noah-MP framework. Maps of all the outputs (runoff, evaporation,

568   groundwater, energy, vegetation) across the grid domain demonstrate consistent spatial patterns that are

569   simulated by the two models. The long-term variations of multiple state variables simulated by the two

570   models also exhibit high consistency, although some differences also exist. By enabling the coupled

571   river routing model~~h on river network~~, the river discharge simulated by NMH-CS 3.0 based on the

572   multiple scheme combination of parameterizations is found to be in reasonable agreement with the

573   reconstructed natural river discharge, for the Lanzhou hydrological station.

574   The main inconsistencies in multiple variables between NMH-CS output and WRF-Hydro output was

575   found to be related to inconsistent judgments on the presence of snow layers, which are caused by

576   minor cumulative errors near the threshold value of 0.025m for snow depth. Overall, while there are

577   occasional~~ly happened~~ disparities between the models' outputs ~~in the NMH-CS simulated results when~~

578   ~~compared to the original WRF-Hydro~~, it reproduces highly consistent spatiotemporal distribution of

579   multiple variables ~~as that by WRF-Hydro 3.0~~. It can therefore be asserted that NMH-CS can be

580   considered a reliable replica of Noah-MP in the uncoupled WRF-Hydro 3.0.

581   This new software NMH-CS can run on Windows system platforms. Its C# code can be analyzed and

582   visually browsed using many modern intelligent tools such as those in Sharpdevelop or Microsoft Visual

583   Studio. This feature makes the code easier to analyze and modify, which in turn will attract more users

584   and promote the future development of the Noah-MP model. The current version of NMH-CS can serve

585   as a good model for simulating land surface processes in climate change and ecohydrology research.

586   Although NMH-CS cannot be used as a coupling module to other FORTRAN based framework models

587   (such as the WRF model), it can still be used as a prototype system to improve the Noah-MP schemes.

588   Any new improvements in NMH-CS can easily be updated to other FORTRAN based Noah-MP.

589   Future plans for the development of NMH-CS include (1) providing a single-column run mode and

590   incorporating a genetic algorithm-based parameter optimization module; (2) extending the functionality

591   for modelling dynamic vegetation by designing new schemes or optimizing parameters; (3)

592   implementing major improved model physics that exists in later versions (for example the Noah-MP 5.0)

593   of Noah-MP into the NMH-CS framework; (4) enabling the functionality of running on UNIX-like

594   systems.

595

596   *Acknowledgements.* Thanks Pei-Rong Lin for her great efforts in guiding Yong-He Liu through the

597   intricacies of Noah-MP.

598

599   *Code and data availability.* 1. The NMH-CS model code is available at

600   https://doi.org/10.57760/sciencedb.16102 (Liu, 2024a). 2. The Noah-MP technical documentation is

601   available at the same site and more details will continue to be added in the documentation. 3. The

602   benchmark meteorological datasets for driving NMH-CS and WRF-Hydro 3.0 were uploaded to the

603   Science Data Bank (DOI: https://doi.org/10.57760/sciencedb.13122 (Liu, 2024b)).

604

Author contributions. Yong-He Liu has translated the code of WRF-Hydro/Noah-MP to NMH-CS, the debugging and the benchmark model simulations. The work is led by Zong-Liang Yang. Liu has drafted the paper, with improvement made by Yang.

Competing interests. The contact author has declared that none of the authors has any competing interests.

Financial support. This study is jointly funded by the "Double First Class" Discipline Construction Project of Surveying and Mapping Science and Technology at Henan University of Technology (GCCYJ202418); Henan Provincial Natural Science Foundation Project (No. 252000421467) and Henan Provincial Key Science and Technology Project (No. 252102320004). This work is funded by the Project on the Creation of "Double First-class" Disciplines in Surveying and Mapping Science and Technology (Grant No. GCCYJ202418), Henan Polytechnic University.

References

Bales, J.: Featured Collection Introduction: National Water Model II, J. Am. Water Resour. As., 55(4), 938-939, https://doi.org/10.1111/1752-1688.12786, 2019.

Biswa, K., Jamatia, B., Choudhury, D. and Borah, P.: Comparative Analysis of C , FORTRAN , C # and Java Programming Languages, ternational Journal of Computer Science and Information Technologies, 7(2), 1004-1007, 2016.

Chang, M., Liao, W., Wang, X., Zhang, Q., Chen, W., Wu, Z. and Hu, Z.: An optimal ensemble of the Noah-MP land surface model for simulating surface heat fluxes over a typical subtropical forest in South China, Agr. Forest Meteorol., 281, https://doi.org/10.1016/j.agrformet.2019.107815, 2020.

Chen, F., Manning, K.W., LeMone, M.A., Trier, S.B., Alfieri, J.G., Roberts, R., Tewari, M., Niyogi, D., Horst, T.W., Oncley, S.P., Basara, J.B. and Blanken, P.D.: Description and evaluation of the characteristics of the NCAR high-resolution land data assimilation system, J. Appl Meteorol Clim, 46(6), 694-713, https://doi.org/10.1175/JAM2463.1, 2007.

Cunge, J. A. On The Subject Of A Flood Propagation Computation Method (Musklngum Method). *Journal of Hydraulic Research*, 7(2), 205–230. https://doi.org/10.1080/00221686909500264, 1969. Cunge, J.A., 1969. On the subject of a flood propagation computation method (Muskingum method). Journal of Hydraulic Research.

David, C.H., Yang, Z. and Famiglietti, J.S.: Quantification of the upstream-to-downstream influence in the Muskingum method and implications for speedup in parallel computations of river flow, Water Resour. Res., 49(5), 2783-2800, https://doi.org/10.1002/wrcr.20250, 2013.

David, C.H., Famiglietti, J.S., Yang, Z. and Eijkhout, V.: Enhanced fixed-size parallel speedup with the Muskingum method using a trans-boundary approach and a large subbasins approximation, Water Resour. Res., 51(9), 7547-7571, https://doi.org/10.1002/2014WR016650, 2015.

Francesca, V., Kelly, M., Laura, R., Fernando, S., Bradford, B., Jason, E., Brian, C., Aubrey, D., David, G. and Robert, C.: A Multiscale, Hydrometeorological Forecast Evaluation of National Water Model Forecasts of the May 2018 Ellicott City, Maryland, Flood, J. Hydrometeorol., 21(3), 2020.

Gan, Y., Liang, X., Duan, Q., Chen, F., Li, J. and Zhang, Y.: Assessment and Reduction of the Physical Parameterization Uncertainty for Noah-MP Land Surface Model, Water Resour. Res., 55(7), 5518-5538, https://doi.org/10.1029/2019WR024814, 2019.

Gao, Y., Li, K., Chen, F., Jiang, Y. and Lu, C.: Assessing and improving Noah-MP land model simulations for the central Tibetan Plateau, J. Geophys. Res.-Atmos., 120(18), 9258-9278, https://doi.org/10.1002/2015JD023404, 2015.

Gochis, D.J., W. Yu, D.N. Yates, 2015: The WRF-Hydro model technical description and user's guide, version 3.0. NCAR Technical Document. 123 pages.

Gochis, D.J.A.C., 2020. The WRF-Hydro modeling system technical description (version 5.1.1). NCAR Tech. Note.

He, C., Valayamkunnath, P., Barlage, M., Chen, F., Gochis, D., Cabell, R., Schneider, T., Rasmussen, R., Niu, G.Y., Yang, Z.L., Niyogi, D. and Ek, M.: Modernizing the open-source community Noah with multi-parameterization options (Noah-MP) land surface model (version 5.0) with enhanced modularity, interoperability, and applicability, Geosci Model Dev, 16(17), 5131-5151, https://doi.org/10.5194/gmd-16-5131-2023, 2023.

Karki, R., Krienert, J.M., Hong, M. and Steward, D.R.: Evaluating Baseflow Simulation in the National Water Model: A Case Study in the Northern High Plains Region, USA, J. Am. Water Resour. As., 57(2), 267-280, https://doi.org/10.1111/1752-1688.12911, 2021.

Kumar, S.V., Peters-Lidard, C.D., Tian, Y., Houser, P.R., Geiger, J., Olden, S., Lighty, L., Eastman, J.L., Doty, B., Dirmeyer, P., Adams, J., Mitchell, K., Wood, E.F. and Sheffield, J.: Land information system: An interoperable framework for high resolution land surface modeling, Environ. Modell. Softw., 21(10), 1402-1415, https://doi.org/https://doi.org/10.1016/j.envsoft.2005.07.004, 2006.

Li, J., Miao, C.Y., Zhang, G., Fang, Y.H., Wei, S.G. and Niu, G.Y.: Global Evaluation of the Noah-MP Land Surface Model and Suggestions for Selecting Parameterization Schemes, J. Geophys. Res.-Atmos., 127(5), https://doi.org/10.1029/2021JD035753, 2022.

Liang, X., Lettenmaier, D.P., Wood, E.F. and Burges, S.J.: A simple hydrologically based model of land surface water and energy fluxes for general circulation models, Journal of Geophysical Research: Atmospheres, 99(D7), 1994.

Lin, P., Yang, Z., Gochis, D.J., Yu, W., Maidment, D.R., Somos-Valenzuela, M.A. and David, C.H.: Implementation of a vector-based river network routing scheme in the community WRF-Hydro modeling framework for flood discharge simulation, Environ. Modell. Softw., 107, 1-11, https://doi.org/10.1016/j.envsoft.2018.05.018, 2018.

Liu, Y.: Source code for NMH-CS 1.0, Science Data Bank, https://doi.org/10.57760/sciencedb.16102, 2024a.

Liu, Y.: A 3-hourly meteorological forcing dataset for land surface modeling for the Yellow River Basin and North China, Science Data Bank, https://doi.org/10.57760/sciencedb.13122, 2024b.

Liu, Y., Yang, Z. and Lin, P.: Parallel river channel routing computation based on a straightforward domain decomposition of river networks, J. Hydrol., 625, https://doi.org/10.1016/j.jhydrol.2023.129988, 2023.

Ma, N., Niu, G., Xia, Y., Cai, X., Zhang, Y., Ma, Y. and Fang, Y.: A Systematic Evaluation of Noah-MP in Simulating Land-Atmosphere Energy, Water, and Carbon Exchanges Over the Continental United States, J. Geophys. Res.-Atmos., 122(22), 12245-12268, https://doi.org/10.1002/2017JD027597, 2017.

Mizukami, N., Clark, M.P., Sampson, K., Nijssen, B., Mao, Y., McMillan, H., Viger, R.J., Markstrom,

S.L., Hay, L.E., Woods, R., Arnold, J.R. and Brekke, L.D.: mizuRoute version 1: a river network routing tool for a continental domain water resources applications, Geosci Model Dev, 9(6), 2223-2238, https://doi.org/10.5194/gmd-9-2223-2016, 2016.

Niu, G., Yang, Z., Mitchell, K.E., Chen, F., Ek, M.B., Barlage, M., Kumar, A., Manning, K., Niyogi, D., Rosero, E., Tewari, M. and Xia, Y.: The community Noah land surface model with multiparameterization options (Noah-MP): 1. Model description and evaluation with local-scale measurements, J. Geophys. Res.-Atmos., 116(D12109), https://doi.org/10.1029/2010JD015139, 2011.

Rodell, M., Houser, P.R., Jambor, U., Gottschalck, J. and Mitchell, K.: The global land data assimilation system, B. Am. Meteorol. Soc., 85(3), 381-394, 2004.

Taylor, K.E.: Summarizing multiple aspects of model performance in a single diagram, Journal of Geophysical Research: Atmospheres, 106(D7), 7183-7192, https://doi.org/https://doi.org/10.1029/2000JD900719, 2001.

Wu, W., Yang, Z. and Barlage, M.: The Impact of Noah-MP Physical Parameterizations on Modeling Water Availability during Droughts in the Texas-Gulf Region, J. Hydrometeorol., 22(5), 1221-1233, https://doi.org/10.1175/JHM-D-20-0189.1, 2021.

Yang, Q., Dan, L., Lv, M., Wu, J., Li, W. and Dong, W.: Quantitative assessment of the parameterization sensitivity of the Noah-MP land surface model with dynamic vegetation using ChinaFLUX data, Agr. Forest Meteorol., 307, https://doi.org/10.1016/j.agrformet.2021.108542, 2021.

Yang, Z., Niu, G., Mitchell, K.E., Chen, F., Ek, M.B., Barlage, M., Longuevergne, L., Manning, K., Niyogi, D., Tewari, M. and Xia, Y.: The community Noah land surface model with multiparameterization options (Noah-MP): 2. Evaluation over global river basins, J. Geophys. Res.-Atmos., 116(D12110), https://doi.org/10.1029/2010JD015140, 2011.

Zheng, H., Yang, Z.L., Lin, P.R., Wei, J.F., Wu, W.Y., Li, L.C., Zhao, L. and Wang, S.: On the Sensitivity of the Precipitation Partitioning Into Evapotranspiration and Runoff in Land Surface Parameterizations, Water Resour. Res., 55(1), 95-111, https://doi.org/10.1029/2017WR022236, 2019.